JOURNAL OF SOLID STATE CHEMISTRY 48, 196–208 (1983)

Lattice Vibration Spectra, XXXIII: Far-Infrared Reflection Spectra, TO and LO Phonon Frequencies, Optical and Dielectric Constants, and Effective Charges of the Spinel-Type Compounds MCr_2S_4 (M = Mn, Fe, Co, Zn, Cd, Hg), MCr_2Se_4 (M = Zn, Cd, Hg), and MIn_2S_4 (M = Mn, Fe, Co, Ni, Cd, Hg)

H. D. LUTZ, G. WÄSCHENBACH, G. KLICHE, AND H. HAEUSELER

Laboratorium für anorganische Chemie der Universität Siegen
Adolf-Reichwein-Straße, D-5900 Siegen, West Germany

Received December 15, 1982

The far-infrared reflection spectra of hot-pressed samples of the spinels MCr_2S_4 with M = Mn, Fe, Co, Zn, Cd, and Hg, MCr_2Se_4 with M = Zn, Cd, and Hg, and MIn_2S_4 with M = Mn, Fe, Co, Ni, Cd, Hg have been recorded in the range from 40 to 700 cm^{-1}. The spectra show four reststrahlen bands in the case of normal spinels and up to five in the case of inverse spinels. The transverse and longitudinal optical phonon frequencies at wave vector $|\mathbf{q}| \simeq 0$ are determined by Kramers–Kronig analysis and the classical oscillator-fit method. Effective ionic charges (normalized splitting, transverse effective charge, Szigeti charge) were calculated from the experimentally determined TO/LO splittings and from the high frequency dielectric constants. The obtained data reveal an increasing covalency of the chalcide spinels in the order selenides > sulfides, chromium compounds > indium compounds, inverse spinels > normal spinels, $NiM^{II}_2X_4 > CoM^{II}_2X_4 > FeM^{II}_2X_4 > MnM^{II}_2X_4$, $HgM^{II}_2X_4 > ZnM^{II}_2X_4 > CdM^{II}_2X_4$.

Introduction

Far-infrared studies on spinel type compounds have been done in the last 15 years in terms of structural investigations, as, for example, cation ordering, lattice dynamical calculations, bonding problems, e.g., bond strengths and ionicities, free carrier contributions, and magnetic phenomena. Although the first infrared spectra of sulfide spinels were already reported in 1966 (*1*), only in the case of a few compounds, viz., MCr_2X_4 with M = Zn, Cd, Hg and X = S, Se (*2–7*) and $CdIn_2S_4$ (*8, 9*), are the TO and LO phonon frequencies and the optical and dielectric constants available in the literature. Because these data are necessary for further work on lattice dynamics and the calculation of effective dynamical charges, we analysed the far-infrared reflection spectra of all chromium and indium chalcide spinels suitable for infrared spectroscopic studies. From the obtained spectra we calculated both the dielectric and optical constants and the transverse and longitudinal optical phonon frequencies (wave vector $|\mathbf{q}| \simeq 0$), with the aid of the classical oscillator method and the Kramers–Kronig analysis. We further intended to study the trends of these data including the effective dynamical charges within the chalcide spinels under investigation.

0022-4596/83 $3.00

Experimental

The spinels were prepared, as described elsewhere (*10, 11*), by firing stoichiometric amounts of the elements or the binary chalcides. The reactions were carried out in sealed, evacuated silica tubes (or in alumina crucibles inserted in silica ampules, for the case of the indium compounds) at 700–900°C for 10–12 days; in the case of $HgCr_2Se_4$ and $HgIn_2S_4$, which tend to decompose at these temperatures, the firings were carried out at 600 and 400°C, respectively.

X-ray Guinier powder technique was used to confirm the structure and the lattice constants of the cubic spinels. The observed lattice constants are in good agreement with literature data.

Pressed pellets of the spinel samples with mirrorlike surfaces were obtained using a hot-pressing technique (*12*). The microcrystalline spinel samples were placed in a die between pistons of graphite or alumina and pressed in an argon atmosphere under a pressure of $5 \cdot 10^7$ Pa at about 700°C for about 7 hr. The pressed pellets were polished using diamond pastes of 6 and 0.5 μm grain size. Pellets of pure $HgIn_2S_4$ were difficult to obtain because of its decomposition into In_2S_3, Hg, and S during hot pressing.

Measurements of the far-infrared reflection spectra at near normal incidence were performed at ambient temperature with a Bruker IFS 114 FT–IR spectrometer in the spectral range from 40 to 700 cm^{-1}. An aluminum mirror was taken as reference.

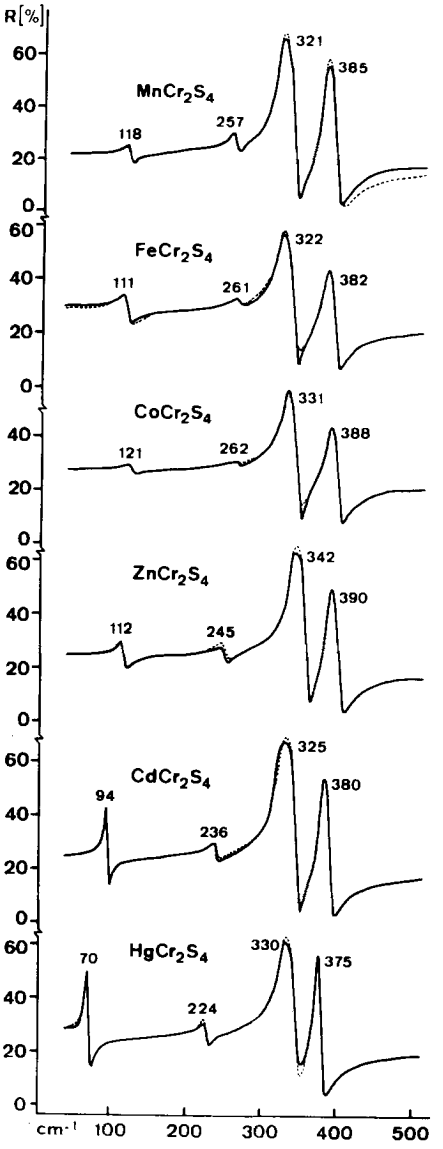

FIG. 1. FIR-reflection spectra of chromium sulfide spinels (dashed lines, oscillator-fit calculations).

Far-Infrared Reflection Spectra

Normal spinels crystallize in the space group $Fd3m$ (O_h^7) with two formula units in the primitive unit cell. Unit cell group analysis according to

$$\Gamma = A_{1g} + E_g + F_{1g} + 3F_{2g} + 2A_{2u} + 2E_u + 4F_{1u} + 2F_{2u}$$

predicts four infrared lattice vibrations of type F_{1u} ($\mathbf{q} = 0$).

Figures 1–3 show the far-infrared reflection spectra of the chalcide spinels under investigation. The reflection spectra of different pellets and different samples of one compound do agree well in their mode frequencies, but differ to some extent in the

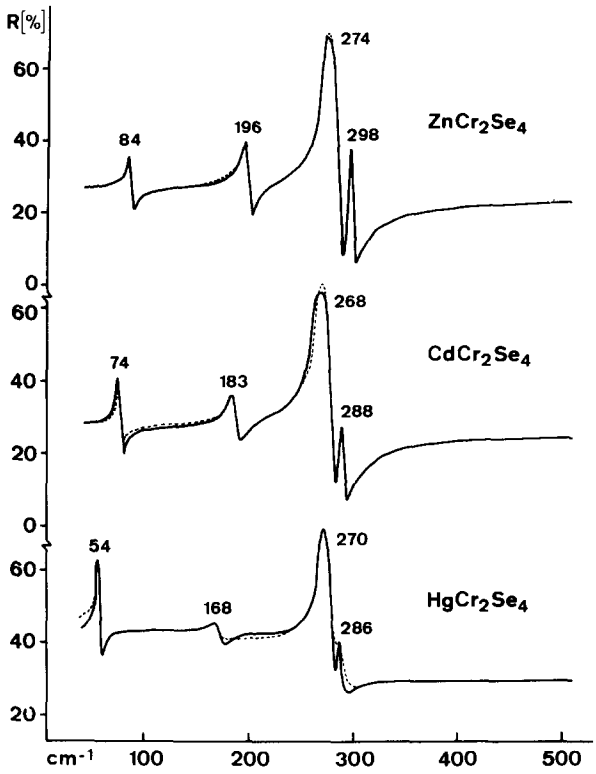

FIG. 2. FIR-reflection spectra of chromium selenide spinels (dashed lines, oscillator-fit calculations).

amount of reflectivity, depending on the surface quality of the obtained pellets.

The spectra of all chromium spinels exhibit the four group-theoretically allowed reststrahlen bands in accordance with the reflection and absorption spectra of these compounds given in the literature (*2–7, 10*); but in the case of $FeIn_2S_4$, $CoIn_2S_4$, and $NiIn_2S_4$, five instead of four phonon frequencies have been found in the reflection spectra (see also *10, 13*), whereas the mainly normal spinel $CdIn_2S_4$ only exhibits four bands (*8, 10, 13*), as predicted for the spinel lattice. In the case of $MnIn_2S_4$ (*10*) and $HgIn_2S_4$ just two reststrahlen bands are observed (see Fig. 3).

Oscillator Fit, Kramers–Kronig Analysis, Oscillator Parameters

From the observed far-infrared spectra, the optical and dielectric constants of the spinels under investigation were calculated using the classical oscillator-fit method and Kramers–Kronig analysis (see Figs. 4 and 5). The details have been reported elsewhere (*14, 15*). The number of oscillators needed to fit the observed reflection spectra depends on the number of reststrahlen bands in the spectra. Therefore, the number of oscillators used varied from two for $MnIn_2S_4$ to five for $FeIn_2S_4$, $CoIn_2S_4$, and $NiIn_2S_4$. The obtained oscillator parameters, i.e., phonon frequencies ω_j, oscillator strengths ρ_j, and damping constant γ_j of the spinels under investigation are compiled in Table I.

In the case of $HgCr_2Se_4$ free carrier contributions must be taken into account, as shown by a broad reflection band in the region from 40 to 500 cm^{-1} (see Fig. 6). The plasma resonance frequencies

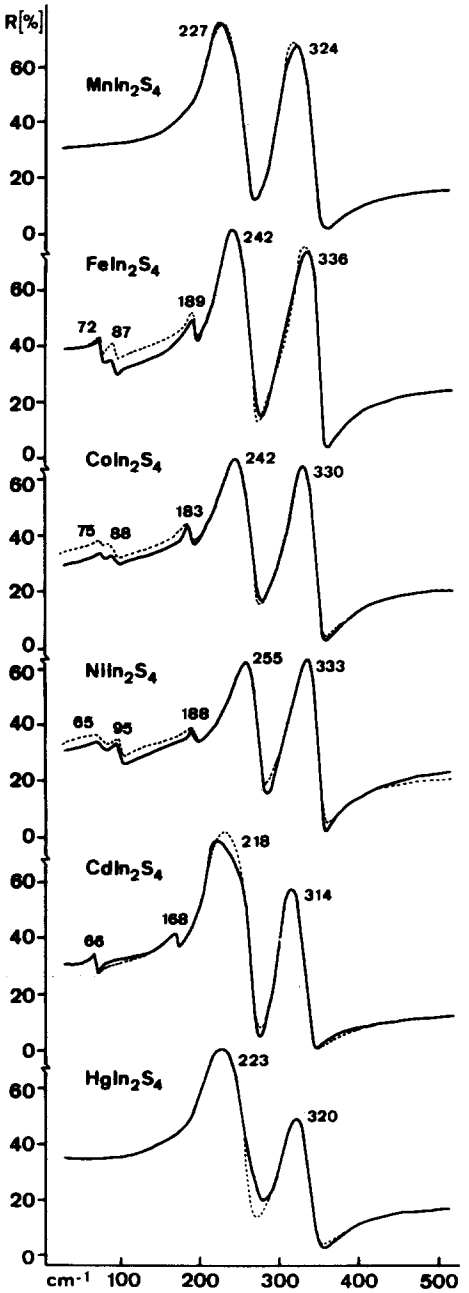

FIG. 3. FIR-reflection spectra of indium sulfide spinels (dashed lines, oscillator-fit calculations).

$$\omega_p' = \left[\frac{4\pi e^2 n_0}{m \cdot \varepsilon_\infty}\right]^{1/2}$$

(n_0 = number of free carriers per unit volume, m = effective mass of the free carriers) of two samples have been calculated to be 277 and 280 cm^{-1}, respectively. The damping of the free carriers is relatively large, i.e., 493 and 567 cm^{-1}, respectively. Plasmon phonon coupling, however, can be neglected in $HgCr_2Se_4$. Detailed studies on the plasmon parameters of $HgCr_2Se_4$ have been carried out by Selmi *et al.* (*5*).

The oscillator strengths of the four reststrahlen bands show some significant features (see Table I) indicating that the eigenvectors of the lattice vibrations differ within the chalcide spinels under investigation. Thus, the relative oscillator strength of the highest wavenumber lattice mode largely decreases on going from the sulfide spinels to the selenide spinels, and from zinc to the mercury compounds, whereas the oscillator strength of the lowest wavenumber mode increases on going from $ZnCr_2S_4$ to $HgCr_2S_4$ and alters discontinuously for the spinels $MnCr_2S_4$, $FeCr_2S_4$, and $CoCr_2S_4$.

There are several direct and indirect methods of obtaining the TO and LO phonon frequencies ($|\mathbf{q}| \simeq 0$) cited in the literature for the chalcide spinels. Thus, the transverse optical phonon frequencies ω_{TO} are identified with (i) the frequencies ω_j obtained from oscillator-fit methods, e.g., Refs. (*2–5, 8*), (ii) the peak positions of the imaginary part of dielectric constant ε'', e.g., Ref. (*6, 7*), and (iii) the maximum points of the modulus of the dielectric constant $|\hat{\varepsilon}| = (\varepsilon'^2 + \varepsilon''^2)^{\frac{1}{2}}$, as recommended by Chang *et al.* (*16*). The longitudinal optical phonon frequencies ω_{LO} are determined from (i) the Lyddane–Sachs–Teller relation, e.g., Ref. (*6*), (ii) the zeros of the real part of the dielectric constant ε', the so-called Drude method, e.g., Refs. (*2, 3*), (iii) the peak positions of the imaginary part of

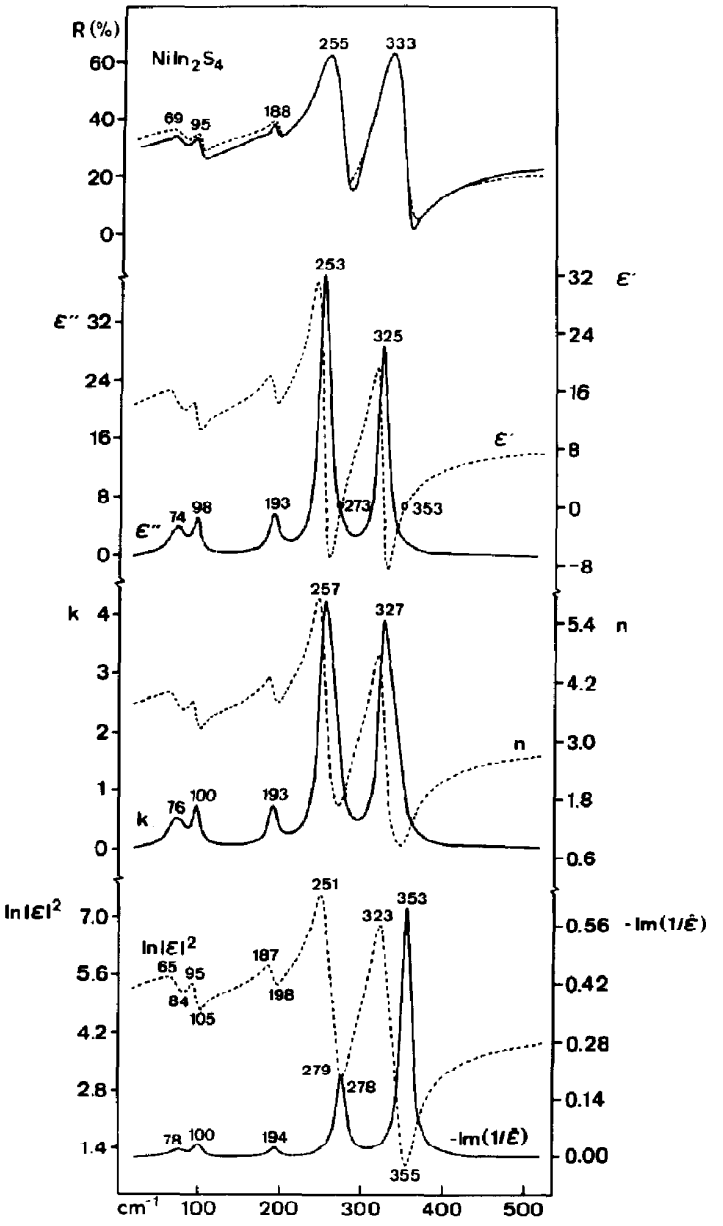

FIG. 4. FIR-reflection spectrum, optical and dielectric functions of $NiIn_2S_4$ calculated by oscillator-fit method.

the inverse dielectric constant $-\mathrm{Im}(1/\hat{\varepsilon}) = \varepsilon''/(\varepsilon'^2 + \varepsilon''^2)$, e.g., Refs. (*4*, *7*, *8*), and (iv) the minimum points of the modulus of the dielectric constant $|\hat{\varepsilon}|$ (*16*).

In determining the TO and LO phonon frequencies of the chalcide spinels under investigation, we found that the observed frequencies differ to some extent according to the method of calculation used. Particularly, the frequencies obtained from the

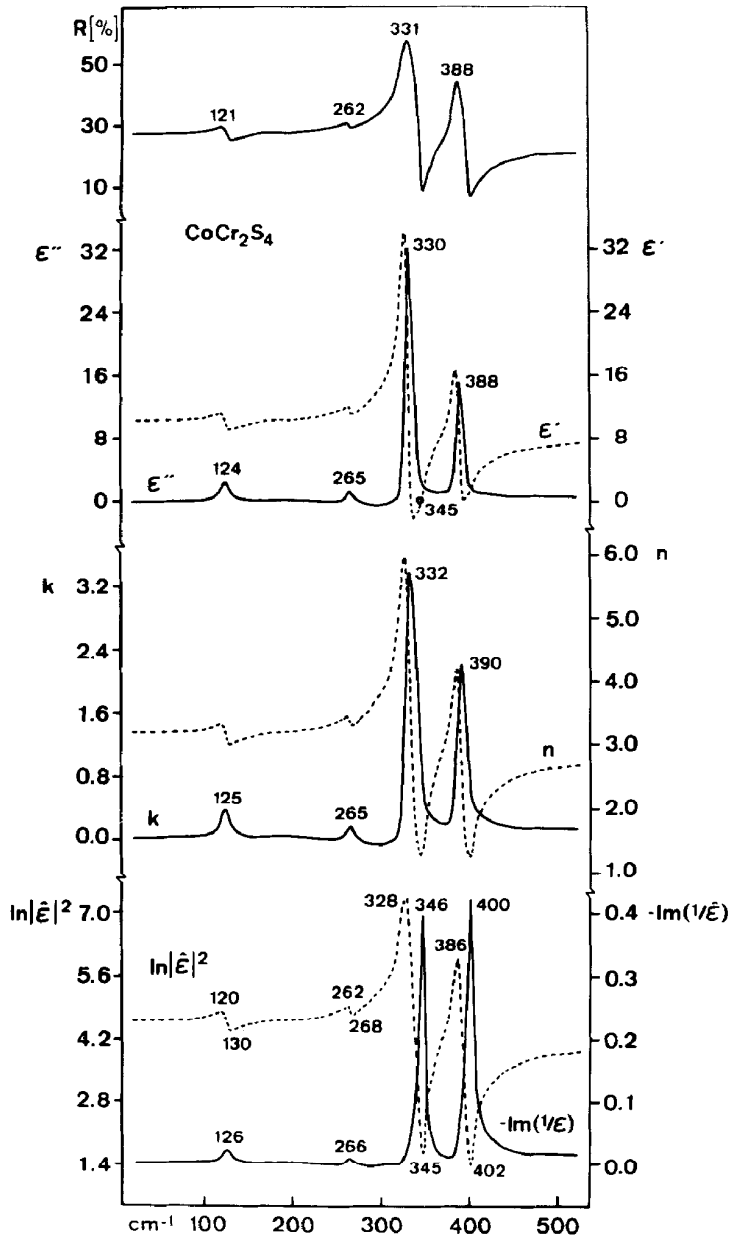

FIG. 5. FIR-reflection spectrum, optical and dielectric functions of $CoCr_2S_4$ calculated by Kramers–Kronig analysis.

maximum and minimum points of the modulus of the dielectric constant $|\hat{\varepsilon}|$ are significantly shifted by about 2 cm^{-1} to lower and higher wavenumbers, respectively, yielding larger TO/LO splittings as compared to that obtained by the other methods (see Figs. 4–6). Experimental features, however, e.g., the different absolute reflectivity of the measured chalcide spinel pellets due to the varying surface quality and the method of

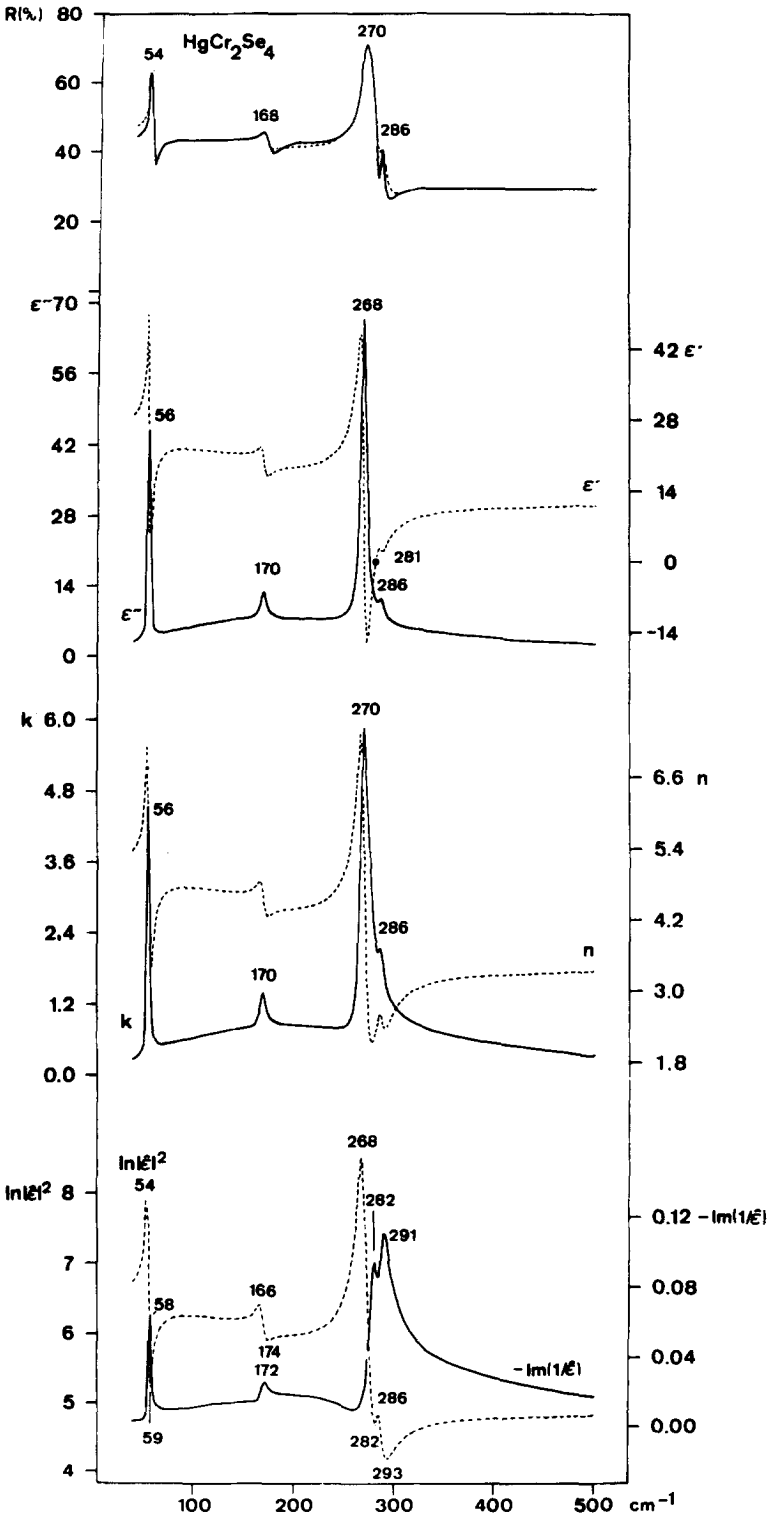

FIG. 6. FIR-reflection spectrum, optical and dielectric functions of $HgCr_2Se_4$ calculated by oscillator-fit method. The free carrier contribution is particularly shown by the function $-\mathrm{Im}1/\hat{\varepsilon}$.

TABLE I

OSCILLATOR PARAMETERS, TO, LO, AND ir ABSORPTION FREQUENCIES (cm^{-1}), AND EFFECTIVE CHARGES[a] OF CHROMIUM AND INDIUM CHALCIDE SPINELS

	j	$4\pi\rho_j$[b]	ω_j[b]	γ_j[b]	ω_{TO}[c]	ω_{LO}[c]	ω_{abs}[d]	Ref.
$MnCr_2S_4$								
ε_∞[b] = 5.9	1	0.36	379	7.6	381	397	382	
Ze^*/e = −0.55	2	1.00	321	8.7	322	342	322	
e_B^*/e = −1.34	3	0.12	261	8.1	262	263	261	
e_S^*/e = −0.51	4	0.17	120	7.3	121	122	121	
$FeCr_2S_4$								
ε_∞ = 8.3	1	0.39	382	10.9	382	396	383	
Ze^*/e = −0.54	2	1.21	321	13.3	321	341	323	
e_B^*/e = −1.56	3	0.04	265	5.2	265	267	259	
e_B^*/e = −0.45	4	0.56	115	11.3	114	118	114	
$CoCr_2S_4$								
ε_∞ = 8.3	1	0.39	387	11.3	388	400	390	
Ze^*/e = −0.48	2	0.99	329	11.8	330	346	332	
e_B^*/e = −1.38	3	0.06	265	14.2	265	266	261	
e_S^*/e = −0.40	4	0.14	124	9.4	124	126	124	
$ZnCr_2S_4$								
ε_∞ = 6.7	1	0.32	387	5.3	388	403	391	
7.5		0.31		6.5	387.0	403.0		(7)
Ze^*/e = −0.55	2	1.07	339	5.7	340	360	341	
−0.58		1.56		7.8	336.0	361.5		(7)
e_B^*/e = −1.42	3	0.14	247	10.6	249	250	246	
		0.21		12.5	247	249.5		(7)
e_S^*/e = −0.49	4	0.29	116	6.4	115	117	114	
−0.50		0.38		7.0	114.5	116.5		(7)
$CdCr_2S_4$								
ε_∞ = 6.9	1	0.29	378	6.4	380	392	381	
7.6		0.27		4.8	378.0	391.0		(7)
6.76		0.29		5.3	378.6	386.6		(6)
7.84		0.31			376.9	389.9		(2)
Ze^*/e = −0.58	2	1.23	325	8.6	324	348	329	
−0.60		1.74		9.2	321.5	350.0		(7)
		1.58		5.4	320.8	356.3		(6)
		1.63			321.6	347.2		(2)
e_B^*/e = −1.52	3	0.13	240	9.6	240	242	239	
		0.21		8.5	239.0	241.0		(7)
		0.20		10.6	240.0	243.5		(6)
e_S^*/e = −0.51	4	0.45	95	2.4	95	98	96	
−0.52		0.56		2.9	95.0	97.5		(7)
		0.47		4.3	96.8	100.1		(6)
$HgCr_2S_4$								
ε_∞ = 7.4	1	0.23	372	4.8	374	384	376	
8.5		0.25		4.4	373.0	384.5		(7)
Ze^*/e = −0.52	2	1.12	329	10.7	332	350	335	
−0.56		1.61		9.0	327.0	350.5		(7)
e_B^*/e = −1.41	3	0.17	228	7.2	228	230	228	
		0.32		10.5	228.0	231.0		(7)
e_S^*/e = −0.45	4	1.06	71	4.4	70	74	82	
−0.46		1.59		3.0	69.5	74.5		(7)

TABLE I—*Continued*

	j	$4\pi\rho_j$[b]	ω_j[b]	γ_j[b]	ω_{TO}[c]	ω_{LO}[c]	ω_{abs}[d]	Ref.
$ZnCr_2Se_4$								
$\varepsilon_\infty = 8.3$	1	0.09	297	3.9	297	302	299	
9.0		0.08		2.8	296.0	300.5		(*4*, *7*)
$Ze^*/e = -0.47$	2	0.96	274	5.8	274	288	280	
-0.48		1.30		5.0	272.5	289.0		(*4*, *7*)
$e_B^*/e = -1.35$	3	0.31	198	6.1	198	201	199	
		0.24		4.5	199.0	201.0		(*4*, *7*)
$e_S^*/e = -0.39$	4	0.33	86	3.1	85	87	88	
-0.40		0.49		5.0	85.5	87.5		(*4*, *7*)
$CdCr_2Se_4$								
$\varepsilon_\infty = 8.9$	1	0.06	288	3.1	288	293	290	
10.2		0.10		4.3	287.0	292.0		(*4*, *7*)
9.0		0.07			288.1	291.4		(*2*)
$Ze^*/e = -0.50$	2	1.06	267	6.9	267	281	271	
-0.50		1.61		4.8	264.0	281.0		(*4*, *7*)
		1.21			266.2	281.3		(*2*)
$e_B^*/e = -1.49$	3	0.23	187	6.2	186	188	185	
		0.23		5.5	187.0	189.0		(*4*, *7*)
$e_S^*/e = -0.41$	4	0.24	75	0.3	75	77	75	
-0.40		0.80		2.9	74.0	76.0		(*4*, *7*)
$HgCr_2Se_4$								
$\varepsilon_\infty = 10.9$	1	0.08	286	6.9	286	291	288	
10.8		0.10		5.0	285.0	290.0		(*4*, *7*)
					286.8	289.9		(*3*)
9.45		0.031		3.8	286			(*5*)
$Ze^*/e = -0.51$	2	1.28	268	6.5	268	282	272	
-0.44		1.19		3.6	270.0	281.0		(*4*, *7*)
					268.6	281.8		(*3*)
		0.96		4.5	269			(*5*)
$e_B^*/e = -1.68$	3	0.22	169	6.6	169	172	170	
		0.35		7.0	170.0	172.0		(*4*, *7*)
$e_S^*/e = -0.39$	4	2.28	55	2.0	55	58	56	
-0.34		0.92		2.6	57.5	60.0		(*4*, *7*)
$MnIn_2S_4$								
$\varepsilon_\infty = 6.0$	1	0.90	309	19.7	307	347	318	
$Ze^*/e = -0.93$	2	4.63	214	21.4	216	265	229	
$e_B^*/e = -2.28$								
$e_S^*/e = -0.85$								
$FeIn_2S_4$								
$\varepsilon_\infty = 7.7$	1	1.02	321	18.9	319	351	327	
$Ze^*/e = -0.83$	2	3.31	232	19.2	230	266	240	
$e_B^*/e = -2.30$	3	0.39	192	6.6	192	194	192	
$e_S^*/e = -0.71$	4	0.40	91	9.1	88	90	91	
	5	0.41	74	5.2	73	75	74	
$CoIn_2S_4$								
$\varepsilon_\infty = 7.9$	1	1.02	319	16.4	319	350	322	
$Ze^*/e = -0.82$	2	3.21	235	21.6	235	270	242	
$e_B^*/e = -2.30$	3	0.46	186	13.4	187	190	186	
$e_S^*/e = -0.70$	4	0.67	91	16.9	92	94	92	
	5	0.52	76	10.5	74	77	75	

TABLE I—*Continued*

	j	$4\pi\rho_j{}^b$	$\omega_j{}^b$	$\gamma_j{}^b$	$\omega_{TO}{}^c$	$\omega_{LO}{}^c$	$\omega_{abs}{}^d$	Ref.
$NiIn_2S_4$								
$\varepsilon_\infty = 8.5$	1	1.20	324	13.6	325	353	330	
$Ze^*/e = -0.74$	2	2.38	253	15.5	253	278	258	
$e_B^*/e = -2.16$	3	0.33	192	12.5	193	194	193	
$e_S^*/e = -0.62$	4	0.40	99	8.9	98	100	98	
	5	0.35	76	25.3	74	78	76	
$CdIn_2S_4$								
$\varepsilon_\infty = 5.8$	1	0.56	304	13.1	306	338	311	
6.6					307	339		(*8*)
6.5					304	336		(*9*)
$Ze^*/e = -0.96$	2	4.56	215	15.5	214	270	232	
					215	270		(*8*)
					208	268		(*9*)
$e_B^*/e = -2.31$	3	0.30	170	8.1	170	172	170	
					171	172		(*8*)
					168	170		(*9*)
$e_S^*/e = -0.89$	4	0.31	69	5.0	69	70	68	
					68	69		(*8*)
$HgIn_2S_4$								
$\varepsilon_\infty = 7.7$	1	0.66	302	39.1	304	338	313	
$Ze^*/e = -0.97$	2	4.70	214	34.9	213	269	241	
$e_B^*/e = -2.69$								
$e_S^*/e = -0.83$								

[a] Effective dynamic charges of S and Se, respectively; "normalized splittings", $Ze^*/e(=\sqrt{S})$; transverse charges, e_B^*/e; Szigeti charges, e_S^*/e (see text).

[b] From oscillator-fit method.

[c] From Kramers–Kronig analysis (see text).

[d] From FIR absorption spectra of microcrystalline samples (Nujol mulls).

calculating the optical and dielectric constants, i.e., oscillator fit or Kramers–Kronig analysis, do not influence the resulting phonon frequencies by more than 1 cm^{-1}.

The TO and LO phonon frequencies of the chalcide spinels under investigation, i.e., mean values of the figures taken from the peak positions of the imaginary part of the dielectric constant ε'' and the inverse dielectric constant -Im $(1/\hat{\varepsilon})$, respectively, are included in Table I, together with literature data. The tabulated phonon frequencies show characteristic shifts within the chalcide spinels studied, confirming the results formerly inferred from the far-infrared absorption spectra (*10*). Thus, the two short waved modes are shifted to higher wavenumbers when going from the manganese to the zinc spinels, and to lower wavenumbers from the zinc to the mercury compounds, with a significant irregularity of ν_2 in the case of $CdCr_2X_4$ (see also (*7*)). The two low wavenumber modes show nonuniform behavior, especially in the series $MnCr_2S_4$ to $ZnCr_2S_4$, indicating that the lattice forces also alter discontinuously within these spinels.

Effective Ionic Charges and the High-Frequency Dielectric Constants

Effective ionic charges calculated from TO/LO splittings of the phonon modes (or

obtained from lattice dynamical calculations, e.g., on the basis of the rigid ion model), have been used in the literature to study the bonding, especially the ionicity, of solid compounds (see, for example, Phillips (*17*)). Different expressions are used in the literature to calculate effective dynamical charges from TO/LO splittings, viz., the so-called normalized splitting (*18*) S, the transverse (or Born) charge $e_B^*/e = \sqrt{S \cdot \varepsilon_\infty}$, the longitudinal (or Callen) charge $e_C^*/e = \sqrt{S/\varepsilon_\infty}$, the Szigeti charge $e_S^*/e = (3e_B^*/e)/(\varepsilon_\infty + 2)$, the localized charge (*19*), and the reduced effective charges, that is, the effective charges divided by the average classical valence Z_{eff}.

Because the normalized splitting S or the effective charge $Ze^*/e(= \sqrt{S}$ (*20*)) are independent of the high-frequency dielectric constant ε_∞, viz.,

$$4\pi^2c^2 \sum_j \omega_{\text{LO}j}^2 - \omega_{\text{TO}j}^2 = \frac{4\pi}{V} \cdot e^2 \cdot Z \left[\frac{n_A(Ze^*/e)_A^2}{m_A} + \frac{n_B(Ze^*/e)_B^2}{m_B} + \frac{n_X(Ze^*/e)_X^2}{m_X}\right]$$

(c = velocity of light, V = volume of the unit cell, e = elementary charge, Z = number of formula units in the cell, n_A, n_B, n_X = stoichiometric coefficients, and m_A, m_B, m_X = atomic masses), many authors used these quantities for studying ionicity trends in solids (see, for example (*22*)). In the case of compounds with dielectric constants > 5 (which indicates that the observed TO/LO splitting is partially caused by the polarizability of the ions involved), the Szigeti charges should be used for studying ionicity effects (*7, 14, 21*), despite the difficulties in determining true values of ε_∞ (see (*14*)).

In the case of ternary compounds, it is not possible to calculate effective charges from TO/LO splittings of the phonon modes alone, i.e., without additional assumptions concerning the charge of one of the atoms

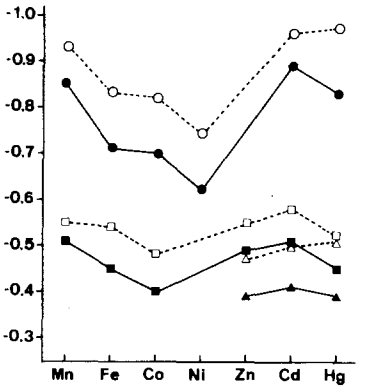

FIG. 7. Szigeti charges e_S^*/e (■, ▲, ●) and the normalized splittings Ze^*/e (= $\sqrt{S}$) (□, △, ○) of chromium sulfide (■, □), chromium selenide (▲, △), and indium sulfide spinels (●, ○).

present (*7, 22*). Values not altered by such additional assumptions are only available by use of lattice dynamical calculations, based on the rigid ion model, for example. To obtain relative effective charges of the nonmetal atoms for studying the ionicities of the spinels under discussion, we set the charge of the bivalent metals to be $\frac{2}{3}$ that of the trivalent ones, i.e., $Ze_A^*/e = \frac{2}{3} \cdot Ze_B^*/e = -Ze_X^*/e$; nevertheless, the effective charges of the nonmetal atoms are only marginally affected by the ratio of the charges chosen for the metal atoms.

The effective dynamical charges of the chalcide spinels, viz., the Szigeti charge e_S^*/e, the transverse charge, e_B^*/e, and the effective charge Ze^*/e obtained under this assumption are included in Table I. As discussed above, the best measure of the ionicity of the spinels under investigation is obviously the Szigeti charge e_S^*/e (or the reduced Szigeti charge $e_S^*/2e$, where 2 is the formal charge of the nonmetal atom).

The following trends of the ionicity of the chalcide spinels can be inferred from the calculated effective charges (see Fig. 7). (i) The ionicity increases when proceeding from the selenide spinels to the sulfides, and when going from the chromium spinels

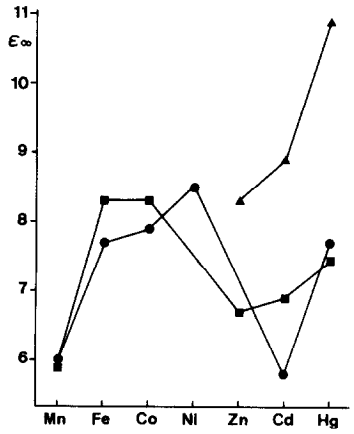

FIG. 8. High frequency dielectric constants ε_∞ of chromium sulfide (■), chromium selenide (▲), and indium sulfide spinels (●).

to the corresponding indium compounds, both in agreement with common chemical sense. (ii) The ionicity decreases in the series from the manganese to the nickel compounds, but then increases strongly when continuing to $ZnCr_2S_4$ and further to $CdCr_2S_4$ or $CdIn_2S_4$, the chalcide spinel with the largest ionicity. It subsequently decreases again on moving to the mercury compounds. These findings are in agreement with results obtained for binary chalcides (*23*) and correlate with the electronegativities of the metal ions. Even the trend of the ionicities of the zinc, cadmium, and mercury compounds is verified if the electronegativity sale of Miedema (*24*) (see also *25*)) is used. (iii) The ionicity of inverse spinels is obviously smaller than that of normal spinels. This is shown by comparing the effective charges of $CoCr_2S_4$ and $HgCr_2S_4$, both normal spinels, and $CoIn_2S_4$ and $HgIn_2S_4$, inverse and normal spinel, respectively.

The high frequency dielectric constants ε_∞ vary for the chalcide spinels under discussion from 5.8 ($CdIn_2S_4$) to 10.9 ($HgCr_2Se_4$) (see Table I). The calculated data reflect the different polarizabilities of the ions involved, e.g., an increase of the polarizability on going from sulfides to selenides and from zinc to mercury compounds (see Fig. 8), as well as the different amounts of covalency in this compounds (with partially delocalized valence electrons). Thus, the covalency of the chalcide spinels increases in the series $MnCr_2S_4 < FeCr_2S_4 < CoCr_2S_4$ and $MnIn_2S_4 < FeIn_2S_4 < CoIn_2S_4 < NiIn_2S_4$, as also shown by the increasing phonon frequencies in the same direction.

Acknowledgments

The authors thank the Deutschen Forschungsgemeinschaft and the Fonds der Chemischen Industrie for financial support.

References

1. H. D. LUTZ, *Z. Anorg. Allg. Chem.* **348,** 30 (1966).
2. T. H. LEE, *J. Appl. Phys.* **42,** 1441 (1971).
3. T. H. LEE, T. COBURN, AND R. GLUCK, *Solid State Commun.* **9,** 1821 (1971).
4. K. WAKAMURA, T. ARAI, AND K. KUDO, *J. Phys. Soc. Japan* **40,** 1118 (1976).
5. A. SELMI, R. LE TOULLEC, AND P. GIBART, *Solid State Commun.* **33,** 889 (1980).
6. M. N. ILIEV AND G. GÜNTHERODT, *Phys. Status Solidi B* **98,** K9 (1980).
7. K. WAKAMURA, T. OGAWA, AND T. ARAI, *Japan J. Appl. Phys.* **19,** 249 (1980).
8. K. YAMAMOTO, T. MURAKAWA, Y. OHBAYASHI, H. SHIMIZU, AND K. ABE, *J. Phys. Soc. Japan* **35,** 1258 (1973).
9. T. G. KERIMOVA, R. KH. NANI, A. SH. KHIDIROV, AND V. YA. SHTEINSHRAIBER, *Izv. Akad. Nauk Az. SSR Ser. Fiz. Tekh. Mat. Nauk* **2,** 52 (1981).
10. H. D. LUTZ AND M. FEHÉR, *Spectrochim. Acta* **27A,** 357 (1971).
11. H. D. LUTZ, W. BECKER, AND W. W. BERTRAM, *J. Solid State Chem.* **37,** 165 (1981).
12. E. CARNALL, D. PEARLMAN, T. J. COBURN, F. MOSER, AND T. W. MARTIN, *Mater. Res. Bull.* **7,** 1361 (1972).
13. H. SHIMIZU, Y. OHBAYASHI, K. YAMAMOTO, AND K. ABE, *J. Phys. Soc. Japan* **38,** 750 (1975).
14. H. D. LUTZ, G. KLICHE, AND H. HAEUSELER, *Z. Naturforsch.* **36a,** 184 (1981).

15. H. D. LUTZ AND G. KLICHE, *Phys. Status Solidi B* **112,** 549 (1982).
16. I. F. CLANY, S. S. MITRA, J. N. PLENDL, AND L. C. MANSUR, *Phys. Status Solidi* **28,** 663 (1968).
17. J. C. PHILLIPS, "Bonds and Bands in Semiconductors," Academic Press, New York (1973).
18. R. M. MARTIN, *Solid State Commun.* **8,** 799 (1970).
19. G. LUKOVSKY, R. M. MARTIN, AND E. BURSTEIN, *Phys. Rev.* **B4,** 1367 (1971).
20. J. F. SCOTT, *Phys. Rev.* **B4,** 1360 (1971).
21. V. P. GUPTA AND V. K. SRIVASTAVA, *J. Phys. Chem. Solids* **42,** 1071 (1981).
22. F. GERVAIS, *Solid State Commun.* **18,** 191 (1976).
23. P. LAWAETZ, *Phys. Rev. Lett.* **26,** 697 (1971).
24. R. BOOM, F. R. DE BOER, AND A. R. MIEDEMA, *J. Less-Common. Met.* **46,** 271 (1976).
25. A. N. BLOCH AND G. C. SCHATTEMAN, *in* "Structure and Bonding in Crystals" (M. O'Keeffe and A. Navrotsky, Eds.), Vol. I, p. 49, Academic Press, New York (1981).